Title

Use of Bender Elements to Evaluate Linkages between Thermal Volume Changes and Shear Modulus Hardening in Drained and Undrained Thermal Triaxial Tests

Journal

Geotechnical Testing Journal, 47(2)

ISSN

0149-6115

Authors

Samarakoon, Radhavi A
Kreitzer, Isaac L
McCartney, John Scott

Publication Date

2024-03-01

DOI

10.1520/gtj20220159

Peer reviewed

Use of bender elements to evaluate linkages between thermal volume changes and shear modulus hardening in drained and undrained thermal triaxial tests

Radhavi A. Samarakoon, Ph.D.

Graduate Research Assistant, Department of Structural Engineering, University of California San Diego, La Jolla, CA 92093-0085, USA; Email: rabeysir@eng.ucsd.edu

Isaac L. Kreitzer, B.S.

Graduate Research Assistant, Department of Structural Engineering, University of California San Diego, La Jolla, CA 92093-0085, USA; Email: ikreitzer@ucsd.edu

John S. McCartney, Ph.D., P.E., F.ASCE (Corresponding Author)

Professor, Department of Structural Engineering, University of California San Diego, La Jolla, CA 92093-0085, USA; Email: mccartney@ucsd.edu

Abstract This study investigates linkages between volume change, pore fluid drainage, shear wave velocity, and temperature of soft clays using a thermal triaxial cell equipped with bender elements, a measurement approach that has not been explored widely in past thermo-mechanical studies. Two kaolinite specimens were consolidated mechanically to a normally consolidated state and then subjected to drained and undrained heating-cooling cycles, respectively. After cooling the specimens were subjected to further mechanical consolidation to evaluate changes in apparent preconsolidation stress. Both specimens showed net contractive thermal strains after a heating-cooling cycle and overconsolidated behavior during mechanical compression immediately after cooling. The shear wave velocity increased during drained heating but negligible changes were observed during drained cooling, indicating permanent hardening due to thermal consolidation during the heating-cooling cycle. The shear wave velocity decreased during undrained heating due to a reduction in effective stress associated with thermal pressurization of the pore fluid, but subsequently increased when drainage was permitted at elevated temperature. The shear wave velocity increased slightly during undrained cooling but decreased when drainage was permitted at room temperature. Net increases in small-strain shear modulus of 17 and 11% after heating-cooling cycles under drained and undrained (with drainage after reaching stable temperatures) conditions, respectively, provide further evidence to the potential of thermal soil improvement of normally consolidated clays. Transient changes in shear modulus also highlight the importance of considering drainage conditions and corresponding changes in effective stress state during heating-cooling cycles.

Keywords: thermal volume change, shear wave velocity, shear modulus, bender elements, thermal triaxial cell, normally consolidated clay

1. Introduction

The impact of temperature on the behavior of clay is important to understand in many geotechnical engineering applications but is particularly critical in in-situ heating for soil improvement, also referred to as thermal soil improvement. Thermal soil improvement has been investigated to improve soft clay layers using thermal drains or energy piles (e.g., Abuel-Naga et al. 2006, Pothiraksanon et al. 2010; Samarakoon and McCartney 2020a, 2021; Ghaaowd and McCartney 2021; Ghaaowd et al. 2022). Thermal drains are vertical porous drains (sands or geosynthetic) that include a geothermal heat exchanger and improve soils by providing both a constant temperature and a free drainage boundary condition for thermal consolidation (Samarakoon and McCartney 2022). Energy piles are rigid elements that provide structural support and heat exchange capabilities, and the heat exchange process can be used to enhance the pullout capacity (Ghaaowd et al. 2022). Despite the development of these thermal soil improvement techniques, the mechanisms of thermal soil improvement are still not well understood, including coupled effects of pore fluid pressurization, effective stress changes, shear modulus changes, and volume changes. Accordingly, the objective of this study is to evaluate the impact of drainage conditions and thermo-mechanical loading paths on the thermal volume change and the corresponding changes in the shear modulus of the soil, as well as to evaluate the coupling between thermal pressurization of pore water during undrained heating or cooling, pore water dissipation during drained heating or cooling, and volume change in saturated normally consolidated clay specimens. Further, this study seeks to better understand the transient trends in the important variables during a thermo-mechanical loading path as many previous studies only focused on equilibrium conditions. Information on the transient linkages

between thermo-mechanical loading paths and soil shear modulus will be useful when determining design parameters in a thermal soil improvement application as well as in the design of energy geostructures.

Several researchers have investigated the effect of temperature on soil behavior including volume change, shear strength, stiffness, and hydraulic conductivity. Many of these studies were focused on highly overconsolidated clays. General observations were that volumetric strains during drained heating are expansive and elastic for overconsolidated clays, and that the magnitude of thermoelastic volumetric strains is dependent on the effective stress and the overconsolidation ratio (Baldi et al. 1988; Hueckel and Baldi 1990; Abuel-Naga et al. 2007a). On the other hand, fewer studies have focused on normally consolidated clays. General observations are that drained heating results in plastic contractive volumetric strains whereas undrained heating results in elastic expansion (Hueckel and Baldi 1990; Cekerevac and Laloui 2004; Abuel-Naga et al. 2007a; Uchaipichat and Khalili 2009). The contractile thermal volumetric strains observed during drained heating of normally consolidated clays also leads to an increase in undrained shear strength (Houston et al. 1985; Kuntiwattanakul et al. 1995; Abuel-Naga et al. 2006; Samarakoon et al. 2018, 2022).

The drained shear strength was also observed to increase with temperature as a result of the soil being subjected to a temperature history (Cekerevac and Laloui 2004; Abuel-Naga et al. 2007b). Alsherif and McCartney (2015) noted that temperature effects on the shear strength of soils also indirectly affects the secant Young's modulus in the axial strain range of 1-3%. The small-strain shear modulus, typically corresponding to shear strains less than 0.001%, is an important parameter needed for characterizing the elastic soil behavior related to geotechnical

structures such as foundations, tunnels, pavements, deep excavations, and the soil response during earthquakes (Atkinson and Sallfors 1991; Mair 1993; Ishihara 1996; Atkinson 2000). At very small strains, the stress-strain behavior of soil is linear elastic with constant shear modulus whereas at higher strains, the soil behavior is observed to be non-linear with reductions in shear modulus with increasing strain (Atkinson 2000). The small-strain shear modulus represents the mechanical response of a soil in its intact state and depends on factors such as void ratio, confining stress, and apparent preconsolidation stress (Hardin and Black 1969; Khosravi and McCartney 2012). In geotechnical engineering applications including the use of in-situ heating for soil improvement (Abuel-Naga et al. 2006, Pothiraksanon et al. 2010; Samarakoon and McCartney 2020a, 2021) as well as energy geostructures such as energy foundations and soil borehole thermal energy storage systems (Brandl 2006, Laloui et al. 2006, Stewart et al. 2014, Murphy et al. 2015), it is expected that the void ratio, effective stress, and apparent preconsolidation stress may change, which indicates that the small-strain shear modulus may be a good indicator of the effects of these parameters which may be difficult to measure directly (i.e., the apparent preconsolidation stress). Most existing thermo-mechanical constitutive models assume that the elastic moduli of soil are independent of temperature (Hueckel and Borsetto 1990; Cui et al. 2000; Laloui and Cekerevac 2003). However, considering the effect of temperature on these parameters will allow for better predictions when designing geotechnical structures subjected to temperature fluctuations. Furthermore, geotechnical structures such as pavements and other earthen structures are also subjected to fluctuations in temperature due to climate effects (McCartney and Khosravi 2013; Vahedifard et al. 2020), so an understanding of the effects of temperature on the small-strain shear modulus may be useful in these applications.

A limited number of studies have been conducted on the effect of temperature on the elastic moduli of soil (Young's modulus or shear modulus) defined at strains less than 0.001%. The effect of temperature and thermal cycles on the small-strain shear modulus of saturated lateritic clay were investigated by Bentil and Zhou (2022) using a temperature-controlled oedometer setup equipped with bender elements. It was observed that for a given vertical effective stress, the small-strain shear modulus at 40 °C was lower compared to its value at 5 °C. However, the small-strain shear modulus was found to increase by about 16% for normally consolidated specimens after being subjected to four thermal cycles ranging from 5 – 40 °C. Other have studied the effects of temperature on the secant Young's modulus of soils at higher strains, which can be related to the secant shear modulus via the Poisson's ratio. Kuntiwattanakul et al. (1995) and Cekerevac and Laloui (2004) used triaxial tests to investigate the effects of temperature on the secant Young's modulus of Kaolin clay at larger strains. The secant shear modulus was obtained at a strain of 0.1% in the study by Kuntiwattanakul et al. (1995) for a temperature range of 0 – 90 °C whereas Cekerevac and Laloui (2004) determined the secant Young's modulus for an axial strain of 0.5% at temperatures ranging from 22 – 90 °C. In both studies, the secant Young's modulus was found to increase with increasing temperature. Similar observations were made by Abuel-Naga et al. (2006) for Bangkok clay where the secant modulus was measured at different deviatoric stress ratios corresponding to axial strains between 0.01% and 6%.

The discrepancies observed in the limited data on soil stiffness parameters may arise due to the differences in the stress or strain states, temperatures and drainage conditions used in the studies. For instance, at higher temperatures, the thermal volume change and its effects on soil stiffness can be more significant. On the other hand, heating and shearing under undrained

conditions will lead to generation of excess pore water pressure, reducing the effective stress of the clay which in turn will decrease the shear modulus. Furthermore, measuring the secant modulus at higher strain levels may incorporate thermo-plasticity effects and soil fabric changes. In addition, the elastic moduli of soil may also be dependent on the mechanical and thermal loading paths. For example, Bentil and Zhou (2022) saw a difference of about 8% in the small-strain shear modulus of a saturated lateritic clay specimen subjected to a compression-cooling path vs. a cooling-compression path. Vahedifard et al. (2020) found a negligible change in small-strain shear modulus of a saturated, compacted silt with an increase in temperature of 20 °C but found decreases in small-strain shear modulus during heating of unsaturated, compacted silt with increasing suction. In view of the limited studies available in literature and the inconsistencies observed in reported data, further investigation is required to better understand the effects of temperature on the small-strain elastic moduli of normally consolidated clay. To that end, this study focuses on the effect of a heating-cooling cycle on the volume change and small strain shear modulus of normally consolidated clay using drained and undrained thermal triaxial tests in a cell that incorporates bender elements into the top and bottom platens.

Bender elements are widely used in laboratory testing to measure shear wave velocity in soils and have been integrated into many standard geotechnical laboratory testing devices including triaxial and oedometer cells (Shirley and Hampton 1978; Dyvik and Madshus 1985; Fam and Santamarina 1995; Viggiani and Atkinson 1995; Pennington et al. 2001; Ghayoomi and McCartney 2011). Bender elements are piezoelectric bending actuators which can convert electrical energy to mechanical energy and vice versa. The transmitting element is excited with a small voltage where it generates a bending motion to induce a vertically propagating shear wave (or s-wave)

in a soil layer. The vibration propagating through the soil is detected by the receiver element that outputs a voltage signal. The transmitted and the received waveforms can be used to obtain the shear wave velocity. The shear wave velocity (V_s) is calculated using the time required for the wave to travel from the transmitter to the receiver and the tip-to-tip distance between benders:

$$V_s = \frac{tip-to-tip\ distance}{travel\ time} \quad (1)$$

The small strain shear modulus (G_0) can be obtained using the following relationship where ρ is the total density of the soil (Hardin and Blandford 1989):

$$G_0 = \rho V_s^2 \quad (2)$$

The total density of the soil can be estimated using the following relationship:

$$\rho = \frac{(G_s + Se)\rho_w}{1 + e} \quad (3)$$

where G_s is the specific gravity of the soil, S is the degree of saturation (equal to 1 for the saturated clay in this study), e is the void ratio, and ρ_w is the density of water. The form of Equation (2) indicates that changes in total density of the soil due to thermal volume changes (i.e., changes in void ratio) may affect the value of G_0 calculated from the value of V_s in addition to the changes in tip-to-tip distance associated with the calculation of the value of V_s. Accordingly, thermal volume change and G_0 should be closely linked. The density of water in Equation (3) varies with temperature as follows (Hillel 1981):

$$\rho_w = 1 - 7.37 \times (10^{-6}) \times (T - 4)^2 + 3.79 \times (T^{-8}) \times (T - 4)^3 \quad (4)$$

where ρ_w has units of g/m^3 and T is in °C. While the effects of temperature on ρ_w cancel out in $\rho_w G_s$ in the first term of the numerator in Equation (3), they are still present in the second term of the numerator in Equation (3) and should be included in the calculation of total density. It should be noted that the effects of temperature on the water density are more important in

drained conditions as the water entering or exiting the specimen may have a different density after temperature changes, while in undrained conditions the mass is constant and only the volume of the specimen changes.

Relationships for G_0 such as those developed by Hardin and Black (1969) and Khosravi and McCartney (2012) indicate that G_0 is not only sensitive to the void ratio but also to the effective stress state and preconsolidation stress. For example, these values follow the power law relationship of Hardin and Black (1966) expressed as follows, neglecting the effects of void ratio and overconsolidation ratio:

$$G_0 = AP_{atm}\left(\frac{\sigma'_{mean}}{P_{atm}}\right)^n \quad (5)$$

where σ'_{mean} is the mean effective normal stress, P_{atm} is the atmospheric pressure (101.3 kPa), and A and n are dimensionless fitting parameters. The presence of effective stress in Equation (5) indicates further possible linkages between G_0 and thermal processes as it is well known that heating of saturated normally consolidated clays will lead to thermal pressurization which may change the effective stress state (Uchaipchat and Khalili 2009; Ghaaowd et al. 2017) and the apparent preconsolidation stress (Uchaipichat and Khalili 2009; Samarakoon and McCartney 2020b). As noted, heating and cooling of clays will also result in changes in void ratio (Campanella and Mitchell 1968; Hueckel and Baldi 1990).

Compression wave velocities can be determined using uniaxial piezoelectric actuators in a similar manner to the shear wave velocities from bender elements, by imparting a vertically propagating compressive pulse on a soil layer. However, the compression wave velocity in saturated soils is typically not measured for saturated soils because the pore water has a higher compressive wave velocity than the soil skeleton (Valle-Molina and Stokoe 2012). Consequently,

the changes in compression wave velocity are not examined in this study. Materials tested, experimental procedures and the results of this study are discussed in the following sections.

2. Material and Test Methods

2.1. Material

This study was conducted on Kaolinite clay obtained from M&M Clays Inc. of McIntyre, GA. The properties of the clay are summarized in Table 1, including the compression indices obtained from an isotropic compression test at room temperature. The clay specimens evaluated in this study were prepared by mixing clay powder with deionized water in a commercial planetary mixer to form a slurry with a gravimetric water content of 115%. The slurry was then poured into a steel hollow cylinder of diameter 88.9 mm with porous stones and filter paper placed at the top and bottom. The slurry was first consolidated using a compression frame at a constant rate of 0.04mm/min for 48 hours. Then it was subjected to constant vertical stresses of 26, 52, 103 and 181 kPa in 24 hour-long increments. The sedimented clay layer was extracted and trimmed to a smaller cylindrical specimen with a diameter of 72.4 mm and a height of 73 mm.

2.2. Experimental Set-up

A triaxial cell with a cell pressure capacity of 4 MPa and internal instrumentation obtained from GDS Instruments of Hook, UK was modified to perform temperature-controlled tests. The internal instrumentation includes a linearly variable differential transformer (LVDT) to measure the axial displacement of the specimen (suitable for pressures up to 3500 kPa and a temperature range of -20 to 110 °C), as well as piezoelectric bender elements embedded in the top and bottom caps to measure the compressional and shear wave velocities of the specimen. While the thermal triaxial system has an additional LVDT for measuring the radial displacement of the specimen,

this system could not be effectively mounted to the soft clay specimen, so only the axial deformation was measured, even though Samarakoon et al. (2022) noted that anisotropic thermal volume changes may occur in the clay. A pore water pressure transducer was used to monitor the changes in pore water pressure at the bottom of the specimen. Temperature control was achieved by circulating the cell fluid through a closed-loop copper heat exchanger that was embedded within a Julabo heat pump (model DYNEO DD-600F). The cell fluid was circulated using a high pressure, high temperature, circulating pump used in solar thermal panel applications (model S5 from US Solar Pumps). The closed-loop heat exchanger was connected to the top and bottom of the cell to mix the cell fluid and ensure uniform temperatures within the cell. The triaxial cell and the heat exchanger sections exposed to the environment were covered with insulation. The cell fluid temperature was measured using a thermocouple inserted at the top of the cell. It was assumed that the measured cell fluid temperature is representative of the specimen temperature. The cell and back pressures were controlled using a pressure panel. A picture and schematic of the thermal triaxial system are shown in Figure 1.

It is important to characterize the thermal deflections of the triaxial system during an application of temperatures as the mounts for the LVDT may expand and contract. Machine deflections due to temperature were obtained by using a dummy Aluminum specimen (linear thermal expansion coefficient, α of 2.3 x 10^{-5} m/m°C) of height of 71.2 mm and diameter of 71.11 mm. The aluminum dummy specimen had recesses around the bender elements for protection during the machine deflection tests. The machine deflections for the thermal triaxial system obtained from a test where a heating-cooling cycle was applied to the cell containing the aluminum dummy specimen with incremental temperature changes from 23 to 63 °C are shown

in Figure 2. The maximum temperature applied in the machine deflection test was the same as that used in the tests on soils. The machine deflections were calculated by subtracting the known elastic thermal deflections of the aluminum dummy specimen from the measured LVDT readings (raw displacement in Fig. 2). The machine deflections can then be used to correct the LVDT readings obtained in tests on soils.

2.3. Procedure

The trimmed clay specimen was placed atop the bottom pedestal of the thermal triaxial cell, carefully pushing the bender element in the base pedestal into the soft clay specimen to ensure intimate contact. The specimen was then encased within a Neoflex membrane from Karol Warner. The Neoflex membrane is made from pure latex coated with a layer of neoprene that can be used to temperatures up to 120 °C. The top cap was then carefully pushed into the top of the specimen, taking care that the bender element was aligned with the bottom bender element. After assembly of the internal LVDT and filling of the cell and heat exchange system with water, the specimen was back-pressure saturated by applying cell pressure and back-pressure in stages until the Skempton's pore water pressure parameter B value was at least 0.95. The specimen was then isotropically consolidated in stages to a mean effective stress of 250 kPa, which corresponds to normally-consolidated conditions. After mechanical consolidation, the specimen was subjected to a heating-cooling cycle, then compressed further to high stresses to measure any changes in mean apparent preconsolidation stress.

Two kaolinite specimens were tested in this study: one subjected to a drained heating-cooling cycle and the other subjected to an undrained heating-cooling cycle that included drainage stages after reaching a stable temperature after heating and after cooling, respectively. The purpose of

performing these tests is to evaluate the impact of drainage conditions on the thermal volume change of the soil, and to evaluate the coupling between thermal pressurization of pore water, pore water dissipation, and volume change in the specimens. Schematics of the thermo-mechanical paths for the drained and undrained tests are shown in Figures 3(a) and 3(b), respectively. Both specimens were first consolidated to normally-consolidated conditions (paths A-B and A'-B', respectively). For the specimen with drained heating (path B-C in Fig. 3(a)), the temperature was increased from 23 °C to 63 °C at a rate of 0.3 °C/hr that was sufficient to minimize the generation of thermally-induced excess pore water pressure within the specimen such that no change in mean effective stress occurs. After the temperature and axia displacement of the specimen were confirmed to be stable, the specimen was cooled back to room temperature (path C-D) at the same rate. Following this heating-cooling cycle, the specimen was isotropically compressed to a mean effective stress of 393 kPa (path D-E in Fig. 3(a)).

In the undrained heating-cooling test, drainage valves were closed during heating and cooling and the pore water pressure was measured at the base of the specimen. After stabilization of the pore water pressures during each stage of undrained heating and cooling, drainage was permitted only from the top of the specimen to track dissipation of thermally induced excess pore water pressure at the base. For the specimen with undrained heating (path B'-C' in Fig. 3(b)), the temperature was increased rapidly at a rate of 22 °C/hr to 63 °C from room temperature which was maintained until the thermally induced excess pore water pressure was observed to stabilize (approximately 80 hrs). The top drain valve was then opened to permit the specimen to drain after heating (path C'-D' in Fig. 3(b)). The specimen was then subjected to undrained cooling (path D'-E' in Fig. 3(b)) at the same rate as heating. The top drain valve was then opened again

to permit the specimen to drain after cooling (path E'-F'). Isotropic compression up to a mean effective stress of 393 kPa after a heating-cooling cycle is shown as path F'-G' in Figure 3(b).

The shear wave velocity was determined using bender elements following ASTM D8295-19 as closely as possible, and the shear modulus was calculated from the shear wave velocity and current value of total density using Equation (2). A deviation from the standard is that the specimen height/diameter ratio was 1:1 to facilitate reasonable times for the thermo-hydraulic processes, but different from typical applications of bender elements in triaxial cells, no shear stress was applied in the isotropic tests reported in this study. Shear wave velocity measurements were performed during each stage of testing and were analyzed using the GDS Bender Element Software. A sinusoidal wave with an amplitude of 14 V and excitation frequency 200 kHz was transmitted through the specimen. The arrival time was determined using the position of the first major peak of the received signal. The tip-to-tip distance at a given time was determined based on the initial height of the specimen and the axial displacement measured from the LVDT. Typical transmitted and received shear wave signals from the pair of bender elements in the triaxial cell are shown in Figure 4. Despite the short travel distance in the specimens, clean signals like those shown in Figure 4 were consistently obtained during the tests and no effect of temperature on the bender elements themselves was detected.

3. Experimental Results

3.1. Typical Time Series Results

Time series of axial strain and temperature during the heating-cooling cycles for the two specimens are shown in Figure 5, where compressive strains are defined as positive. The key transition points in these time series are labelled using the same notation as in Figure 3. The

mean effective stress in both specimens at the onset of the heating-cooling phase was p'=250 kPa. The results for the specimen experiencing a drained heating-cooling cycle are shown in Figure 5(a). The axial strain increases to 0.32% as the temperature increases followed by a slight decrease to 0.28% after drained cooling. The fact that thermal axial strains only occur during the applied changes in temperature confirms that the rate of heating used in this test was sufficient for the soil to be fully drained during heating and cooling. The axial strain of 0.28% at the end of the drained heating-cooling cycle confirms permanent contraction of the soil. The results for the specimen experiencing an undrained heating-cooling cycle are shown in Figure 5(b). The axial strain is observed to decrease to -0.32% as the temperature increases, corresponding to undrained expansion. Once the specimen is allowed to drain at the elevated temperature the specimen contracts to an axial strain of 0.23%. This is slightly smaller than the axial strain observed in the test with drained heating. During undrained cooling, the specimen contracts further to an axial strain of 0.47%. Once the specimen is allowed to drain at room temperature, the specimen expands slightly to an axial strain of 0.39%. The thermal axial strain after an undrained heating-cooling cycle with drainage permitted after the heating and cooling stages is 0.39%, which is greater than that observed in the drained heating-cooling cycle. This difference is attributed to the effective stress in the specimen at the onset of drainage.

Time series of excess pore water pressure during the two tests are shown in Figure 6. The excess pore water pressure generated during the test on the specimen with a drained heating-cooling cycle is negligible with fluctuations between 1-2 kPa in Figure 6(a). During undrained heating a much larger thermally induced excess pore water pressure of 218 kPa is generated as observed in Figure 6(b), corresponding to a decrease in mean effective stress. After the specimen

is allowed to drain under elevated temperatures, these pore water pressures dissipate back to zero, corresponding to an increase in effective stress back to the original value. During undrained cooling the excess pore water pressures decrease to -102 kPa, corresponding to an increase in mean effective stress. After the specimen is allowed to drain at room temperature the excess pore water pressures dissipate again back to zero. The temperatures presented were measured using a thermocouple inserted at the top of the cell, and it is assumed that the cell fluid temperature is representative of the specimen temperature (i.e., it is assumed that the temperature is homogeneous throughout the specimen). However, the use of multiple thermocouples in future tests may provide a better estimate of the temperature distribution within the specimen and whether a temperature gradient exists within the specimen due to the high thermal conductivity of the metallic base pedestal.

The axial strains from Figure 5(b) and the excess pore water pressures from Figure 6(b) from the undrained heating-cooling test are shown in Figure 7 to demonstrate the linkage between these variables. This figure is included to confirm that when the temperature is increased or decreased rapidly in undrained conditions, both the axial strains and excess pore water pressures will take some time to stabilize. Uchaipichat and Khalili (2009) observed that during undrained heating, the thermal expansion and decrease in effective stress correspond to movement along a recompression line, but the results in this figure indicate that movement along this recompression line will be a time dependent process.

3.2. Shear Wave Velocity Measurements

The measured shear wave velocities and the corresponding thermal axial strains for the drained and undrained tests are shown in Figures 8(a) and 8(b), respectively. The key transition

points from Figure 3 are labelled in these figures next to the shear wave velocity values for simplicity. For the specimen subjected to a drained heating-cooling cycle, the shear wave velocity increases with temperature by 17 m/s and remained almost constant during cooling. This increase can be attributed to the plastic thermal strains observed in the clay specimen. The results for shear wave velocity and the thermal axial strain for the specimen subjected to an undrained heating-cooling cycle is shown in Figure 8(b). During undrained heating the shear wave velocity is observed to decrease with temperature by 96 m/s. However, during drainage at elevated temperature, the shear wave velocity increases again by 34 m/s. A slight increase in velocity is observed during undrained cooling which again is reduced during drainage after cooling. A net increase of about 12 m/s is observed after the heating-cooling cycle including the drainage stages after each heating and cooling stages. The differences in the initial shear wave velocity of the two specimens are attributed to the differences in the initial conditions of the sedimented specimens, which had slightly different initial void ratios. Despite this difference, the results from the long-duration tests on both specimens follow expectations from our current understanding of thermal volume change and thermal pressurization and provides useful insight into the differences in behavior expected for drained and undrained heating-cooling cycles which is an important aspect to be considered in the design of energy geostructures.

4. Analysis

4.1. Thermal Strains

The change in thermal axial strain with temperature is shown in Figure 9(a) for the drained test and in Figure 9(b) for the undrained test. The key transition points from Figure 3 are labelled in these figures. Compressive strains observed during drained heating and the slight elastic

expansion during cooling agree with the observations made in literature for normally consolidated clays (Hueckel and Baldi 1990; Cekerevac and Laloui 2004; Abuel-Naga et al. 2007a). The net change in axial strain after a drained heating-cooling cycle was 0.28% and was observed to be contractive. The specimen subjected to an undrained heating-cooling cycle also observed a net contraction of 0.39%, which was slightly greater than that obtained from a drained heating-cooling cycle. The dissipation of thermally induced excess pore water pressure during undrained heating and cooling may have contributed to the increase in the axial displacement observed.

The overall time series of axial strain and temperature for the specimen subjected to a drained heating-cooling cycle including the initial and final compression stages are shown in Figure 10(a) and the corresponding compression curve is shown in Figure 10(b). The key transition points from Figure 3(a) are labelled in these figures. The axial strain of the specimen after consolidation under an isotropic load of 250 kPa is 3.3% as shown in Figure 10(a). As a result of being subjected to drained heating, the axial strain of the specimen increases to 3.6% then reduces slightly to 3.5% after drained cooling. After further mechanical compression up to a mean effective stress of 393 kPa, the specimen experienced an axial strain of 4.4%. Overconsolidated behavior can be observed in the compression curve in Figure 10(b) as the specimen is subjected to mechanical compression after a heating-cooling cycle, although the specimen was at a normally consolidated state prior to heating. The specimen regains a normally consolidated state at a higher stress state upon further loading. This stress state can be approximated as 300 kPa although additional data points will provide a more accurate estimate. Nevertheless, this observation conforms the thermal hardening behavior observed in literature

(Hueckel and Borsetto 1990; Abuel-Naga et al. 2007a) where the yield surface expands after a heating-cooling cycle.

The overall time series of axial strain and temperature for the specimen subjected to a undrained heating-cooling cycle including the initial and final compression stages are shown in Figure 11(a) and the corresponding compression curve is shown in Figure 11(b). The key transition points from Figure 3(b) are included in these figures. The time series results of axial strain indicates that the specimen has an axial strain of 3.7% after isotropic consolidation under a mechanical load of 250 kPa. During undrained heating, the axial strain decreases to 3.4% then increases to 3.9% following drainage at elevated temperature. Undrained cooling leads to an increase in axial strain up to 4.2% but then is reduced to 4.1% after drainage at room temperature. The specimen had a final axial strain of 4.4% after being subjected to further mechanical compression up to 393 kPa. The corresponding compression curve is shown in Figure 11(b). Consistent with the observations of Uchaipichat and Khalili (2009), elastic expansion along the recompression line is observed during undrained heating. Similar observations were made by Ghaaowd et al. (2017) during undrained heating of the same kaolinite clay. Upon further mechanical compression after cooling the observed results were similar to those of the specimen subjected to drained heating and cooling, where overconsolidated behavior is observed after cooling. Interestingly, the contraction during undrained cooling is observed to fall onto the same path of the compression curve where the specimen displayed overconsolidated behavior during mechanical compression after cooling. The effective stress is higher during this stage due to the negative excess pore water pressures generated during undrained cooling. However, once the

specimen was allowed to drain, the excess pore water pressures dissipated and the specimen regains its previous stress state.

The compression curves in terms of volumetric strain for the drained and undrained specimens are shown in Figures 12(a) and 12(b), respectively where the volumetric strain was calculated using the axial strain results. The key transition points from Figure 3 are labelled in these figures. Although radial strains are expected to be higher than axial strains because of the specimen preparation process (Samarakoon et al. 2022), a simplified approach assuming isotropic conditions was used to estimate the volumetric strain where the volumetric strain was assumed to be equal to 3 times the measured axial strain.

4.2. Small Strain Shear Modulus Estimates

Calculation of the variations in small-strain shear modulus from the measured shear wave velocity must include the impacts of thermal volume change on the total density. Accordingly, the variations in total density were calculated using Equation (3) by converting the volumetric strains in Figure 12 into void ratio and accounting for the impact of temperature on the water density using Equation (4). In drained conditions, the changes in volume of the specimen will be equal to the volume of water flowing in or out of the specimen as it is water saturated, but the water density will change with temperature. In undrained conditions, the mass of the specimen is constant while the volume of the specimen is measured directly. The calculated total densities for the drained and undrained specimens during the different stages of the test are shown in Figures 13(a) and 13(b), respectively. The key transition points from Figure 3 are included in these figures. The trends in total densities are similar to the trends in the axial strains shown in Figure 8, which implies that including the effect of temperature on the water density in the calculation of

the total density is negligible compared to the effect of thermal volume changes but can be considered for completeness.

The values of G_0 were then calculated for the two specimens using the measured shear modulus and the estimated total density using Equation (2). The calculated changes in G_0 and thermal volumetric strain with temperature for the drained heating-cooling test are shown in Figure 14(a), along with the key transition points from Figure 3(a) shown next to the transitions in G_0. Like the shear wave velocity, the shear strain modulus increases during drained heating but shows no significant change during drained cooling. The thermal volumetric strain after a drained heating-cooling cycle is 0.84% whereas the corresponding increase in small strain shear modulus is 14%. This increase can be attributed to the plastic thermal strains observed and the corresponding increase in density (0.4% increase after a heating-cooling cycle) in the clay specimen (Eq. (2)). Samarakoon et al. (2022) also observed an increase in undrained shear strength in specimens subjected to drained heating. The trends in Figure 14(a) are also similar to trends in G_0 measured for an unsaturated silt during drying and wetting by Khosravi and McCartney (2012) indicating that the permanent change in G_0 could be associated with both the thermal volume change and the change in apparent preconsolidation stress. The calculated values of G_0 and the corresponding thermal volumetric strains for the specimen subjected to an undrained heating-cooling cycle are shown in Figure 14(b), along with the key transition points from Figure 3(b) shown next to the transitions in G_0. Trends like to those observed for shear wave velocity are observed where the small strain shear modulus decreases with temperature during undrained heating then increases during drainage at elevated temperature. An increase in G_0 is observed during undrained cooling then decreases during drainage at room temperature. The

thermal volumetric strain after being subjected to an undrained heating-cooling cycle is 1.2% and G_0 is observed to increase by 9%. Key results from the two tests are summarized in Table 2.

As described previously, the small strain shear modulus is dependent on factors including void ratio, effective confining stress and the apparent preconsolidation stress. When subjected to a heating-cooling cycle, thermally induced changes occur in the clay specimen. In addition, these thermal changes will also depend on the drainage conditions used. In a saturated normally consolidated clay, as investigated in this study, plastic contractive volume changes attributed to the effects of a drained heating cooling cycle. This reduction in void ratio and the densification of the soil will lead to an increase in the small-strain shear modulus. On the other hand, during undrained heating, expansion is observed and the small-strain shear modulus decreases. However, this expansion is thermo-elastic and is recovered during drainage and subsequent cooling where the shear modulus is observed to increase correspondingly. Furthermore, the generation of excess pore water pressure during undrained heating will decrease the effective stress within the clay specimen. This decrease in effective stress will also contribute to the reduction in the small strain shear modulus according to Equation (5). This indicates the importance of the changes in effective stress due to thermal pressurization on the value of G_0, as the impacts of permanent thermal volume change and changes in apparent preconsolidation stress are not expected to occur until drainage is permitted. On the other hand, during undrained cooling, the negative pore water pressures generated increases the effective stress of the specimen. Accordingly, an increase can be observed in the small strain shear modulus. When drainage is permitted, the pore pressures dissipated and the shear modulus is seen to reduce. Under both drainage conditions, after being subjected to a heating-cooling cycle, an increase in

the apparent preconsolidation stress of the clay was observed in Figures 10 through 12. Due to thermal hardening of the clay, the elastic domain is expanded where the initially normally-consolidated specimen behaves as an overconsolidated specimen immediately after a heating-cooling cycle. This increase in the apparent preconsolidation stress is another contributing factor to the changes in the small-strain shear modulus observed.

As mentioned, the tests presented in this study are time consuming and complex. Although only two tests are considered in this paper, the data presented has value in understanding the impacts of drainage conditions on soil thermo-mechanical behavior. Further testing is needed to better understand the effect of different specimen conditions and to understand uncertainty. Based on the results of this study, some useful insights can be drawn with respect to the thermal volume change and pressurization behavior of clay and their linkages with stiffness characteristics. This information is beneficial in geotechnical applications involving thermal loading such as the use of in-situ heating for soil improvement. The experimental approach described herein has not been used to study the different mechanisms of soil behavior during heating-cooling cycles with different drainage conditions, and only a limited number of studies have been performed on the thermal effects on small-strain shear modulus. Further investigations considering different conditions (i.e., stress states, initial void ratios, temperature ranges, rate of heating, soil types, etc.) will help enhance the understanding of the thermal effects on small-strain shear modulus.

5. Conclusion

This study presents the results of an experimental investigation where the transient linkages between thermal volume change and small-strain shear modulus were evaluated for two

normally consolidated kaolinite specimens subjected to drained and undrained heating-cooling cycles, respectively. In the specimen undergoing a drained heating-cooling cycle, the rates of heating and cooling were sufficiently slow to minimize the generation of thermally induced excess pore water pressures. In the specimen undergoing undrained heating and cooling, drainage was permitted after reaching thermo-hydraulic equilibrium at the end of cooling. In both specimens, net contractive thermal strains were observed at the end of the heating-cooling cycle with slightly higher strains obtained for the specimen subjected to the undrained heating-cooling cycle. Upon further mechanical compression after cooling, both specimens exhibited overconsolidated behavior, even though the specimens were at a normally consolidated state prior to heating. The shear wave velocity was observed to increase with temperature during drained heating and remained constant during drained cooling, leading to a net increase in shear wave velocity after the heating-cooling cycle. On the other hand, shear wave velocity was observed to decrease dramatically during undrained heating due to the increase in thermally induced pore water pressure followed by an increase during drainage at elevated temperature. During undrained cooling, a slight increase in velocity was observed with a subsequent reduction during drainage after cooling, but still resulting in a net increase in shear wave velocity after the heating-cooling cycle. The changes in small strain shear modulus calculated using the change in volume of the specimens were also observed to follow a similar trend to that of shear wave velocity for the kaolinite specimens. A net increase in small-strain shear modulus was observed in specimens after a heating-cooling cycle which can be attributed to the contractive thermal volume changes and the thermal hardening associated with the increase in preconsolidation stress observed in normally consolidated clay. Overall, the methodology and experimental

approach presented in this study can be used to better understand the effects of thermal improvement of soft clays.

Acknowledgements

Funding from NSF grant CMMI 1941571 is appreciated. The opinions are those of the authors.

References

Abuel-Naga, H.M., Bergado, D.T., Chaiprakaikeow, S. (2006). "Innovative thermal technique for enhancing the performance of prefabricated vertical drain during the preloading process." *Geotextiles and Geomembranes*. 24, 359-370.

Abuel-Naga, H.M., Bergado, D.T., Bouazza, A., Ramana, G.V. (2007a). "Volume change behaviour of saturated clays under drained heating conditions: experimental results and constitutive modeling." *Canadian Geotechnical Journal*. 44, 942-956.

Abuel-Naga, H.M., Bergado, D.T., Bee, F.L. (2007b). "Effect of temperature on shear strength and yielding behavior of soft Bangkok clay." *Soils and Foundations*. 47(3), 423-436.

Alsherif, N.A., McCartney, J.S. (2015). "Thermal behaviour of unsaturated silt at high suction magnitudes." Géotechnique. 65(9), 703-716. DOI: 10.1680/geot./14.P.049.

Atkinson, J.H., Sallfors, G. (1991). "Experimental determination of soil properties." General Report to Session 1. *Proceedings of the 10th ECSMFE*. Florence. 3, 915-956.

Atkinson, J.H. (2000). "Non-linear soil stiffness in routine design." *Géotechnique*. 50(5), 487-508.

Baldi, G., Hueckel, T., Pellegrini, R. (1988). "Thermal volume changes of mineral-water system in low-porosity clay soils." *Canadian Geotechnical Journal*. 25, 807-825.

Bentil, O.T., Zhou, C. (2022). “Effects of temperature and thermal cycles on the elastic shear modulus of saturated clay.” *Journal of Geotechnical and Geoenvironmental Engineering*. 148(7), 06022006.

Brandl, H. (2006). “Energy foundations and other thermo-active ground structures.” *Géotechnique*. 56(2), 81-122.

Campanella, R.G., Mitchell, J.K. (1968). “Influence of temperature variations on soil behavior.” *Journal of the Soil Mechanics and Foundation Division. ASCE*. 94(3), 709-734.

Cekerevac, C., Laloui, L. (2004). “Experimental study of thermal effects on the mechanical behaviour of a clay.” *International Journal for Numerical and Analytical Methods in Geomechanics*. 28, 209-228.

Cui, Y.J., Sultan, N., Delage, P. (2000). “A thermomechanical model for clays.” *Canadian Geotechnical Journal*. 37(3), 607-620.

Dyvik, R., Madshus, C. (1985). “Lab measurements of G_{max} using bender elements.” *Norwegian Geotechnical Institution Publication*. Report No. 161, Oslo.

Fam, M., Santamarina, C. (1995). “Study of geoprocesses with complementary mechanical and electromagnetic wave measurements in an oedometer.” *Geotechnical Testing Journal*. 18(3), 307-314.

Ghaaowd, I., Takai, A., Katsumi, T., McCartney, J.S. (2017). “Pore water pressure prediction for undrained heating of soils.” *Environmental Geotechnics*. 4(2), 70-78.

Ghaaowd, I., McCartney, J.S., and Saboya, Jr., F. (2022). “Centrifuge modeling of temperature effects on the pullout capacity of torpedo piles in soft clay.” Soils and Rocks. 45(1), e2022000822. DOI: 10.28927/SR.2022.000822.

Ghaaowd, I., McCartney, J.S. (2021). "Centrifuge modeling methodology for energy pile pullout from saturated soft clay." ASTM Geotechnical Testing Journal. 45(2), 332-354. DOI: 10.1520/GTJ20210062.

Ghayoomi, M., McCartney, J.S. (2011). "Measurement of small-strain shear moduli of partially saturated sand during infiltration in a geotechnical centrifuge." *Geotechnical Testing Journal*. 34(5), 1-11.

Hardin, B.O., Black, W.L. (1969). "Closure to vibration modulus of normally consolidated clays." *Journal of Soil Mechanics and Foundations Division. ASCE.* 95(6), 1531–1537.

Hardin, B.O., Blandford, G.E. (1989). "Elasticity of Particulate Materials." *Journal of Geotechnical Engineering.* 115(6), 788–805.

Hillel, D. (1980), *Fundamental of Soil Physics*, Academic, San Diego, Calif.

Houston, S.L., Houston, W.N., Williams, N.D. (1985). "Thermo-mechanical behavior of seafloor sediments." *Journal of Geotechnical Engineering*. 111(12), 1249-1263.

Hueckel, T., Baldi, M. (1990). "Thermoplasticity of saturated clays: Experimental constitutive study." *Journal of Geotechnical Engineering*. 116(12), 1778-1796.

Hueckel, T., Borsetto, M. (1990). "Thermoplasticity of saturated soils and shales: constitutive equations." *Journal of Geotechnical Engineering*. 116(12), 1765-1777.

Ishihara, K. (1996). *Soil behaviour in earthquake geotechnics.* Oxford University Press.

Khosravi, A., McCartney, J.S. (2012). "Impact of hydraulic hysteresis on the small-strain shear modulus of low plasticity soils." *Journal of Geotechnical and Geoenvironmental Engineering*. 138(11), 1326–1333.

Kuntiwattanakul, P., Towhata, I., Ohishi, K., Seko, I. (1995). "Temperature effects on undrained shear characteristics of clay." *Soils and Foundation*. 35(1), 147-162.

Laloui, L., Cekerevac, C. (2003). "Thermo-plasticity of clays: an isotropic yield mechanism." *Computers and Geotechnics*. 30(8), 649-660.

Laloui, L., Nuth, M., Vulliet, L. (2006). "Experimental and numerical investigations of the behaviour of a heat exchanger pile." *International Journal for Numerical and Analytical Methods in Geomechanics*. 30(8), 763-781.

Mair, R.J. (1993). "Developments in geotechnical engineering research: applications to tunnels and deep excavations. Unwin Memorial Lecture 1992." *Proceedings of the Institution of Civil Engineers – Civil Engineering*. 97(1), 27-41.

McCartney, J.S., Khosravi, A. (2013). "Field monitoring system for suction and temperature profiles under pavements." *Journal of Performance of Constructed Facilities*. 27(6), 818-825.

Murphy, K.D., McCartney, J.S., Henry K.H. (2015). "Thermo-mechanical response tests on energy foundations with different heat exchanger configurations." *Acta Geotechnica*. 10(2), 179-195.

Pennington, D.S., Nash, D.F.T., Lings, M.L. (2001). "Horizontally mounted bender elements for measuring anisotropic shear moduli in triaxial clay specimens." *Geotechnical Testing Journal*. 24(2), 133-144.

Pothiraksanon, C., Bergado, D.T., Abuel-Naga, H.M. (2010). "Full-scale embankment consolidation test using prefabricated vertical thermal drains." *Soils and Foundations*. 50(5), 599-608.

Samarakoon, R.A., Ghaaowd, I., McCartney, J. S. (2018). "Impact of drained heating and cooling on undrained shear strength of normally consolidated clay." *Proc. 2nd International Symposium on Energy Geotechnics*. Lausanne. A. Ferrari, L. Laloui, eds., Vienna. 243-249.

Samarakoon, R.A., McCartney, J.S. (2020a). "Analysis of thermal drains in soft clay." *GeoAmericas 2020. 4th PanAm Conference on Geosynthetics.* Rio de Janeiro, Brazil. Oct. 26-31. 1-9.

Samarakoon, R.A., McCartney, J.S. (2020b). "Effect of drained heating and cooling on the preconsolidation stress of saturated normally consolidated clays." *GeoCongress 2020*. GSP 315. Minneapolis, MN. ASCE. Feb. 25-28. 620-629.

Samarakoon, R.A., McCartney, J.S. (2021). "Performance of prefabricated thermal drains in soft clay." *Geosynthetics Conference 2021*. Kansas City, MO, USA. Feb. 21-24. Nicks, J. and Beauregard, M., eds. IFAI, Roseville, MI. 1-12.

Samarakoon, R., McCartney, J.S. (2022). "Simulation of thermal drains using a new constitutive model for thermal volume change of normally consolidated clays." *Computers and Geotechnics*. 153, 105100.

Samarakoon, R.A., Kreitzer, I.L., McCartney, J.S. (2022). "Impact of initial effective stress on the thermo-mechanical behavior of normally consolidated clay." *Geomechanics for Energy and the Environment*. 32. 100407.

Shirley, D.J., Hampton, L.D. (1978). "Shear-wave measurements in laboratory sediments." *The Journal of the Acoustical Society of America*. 63(2), 607-613.

Stewart, M.A., McCartney, J.S. (2014). "Centrifuge modeling of soil-structure interaction in energy foundations." *Journal of Geotechnical and Geoenvironmental Engineering*. 140(4), 04013044.

Uchaipichat, A., Khalili, N. (2009). "Experimental investigation of thermo-hydro-mechanical behaviour of an unsaturated silt." *Géotechnique*. 59(4), 339–353.

Vahedifard, F., Cao, T.D., Thota, S.K., Samarakoon, R.A., McCartney, J.S. (2020). "A temperature-dependent model for small-strain shear modulus of unsaturated soils." ASCE Journal of Geotechnical and Geoenvironmental Engineering. 146(12), 04020136.

Valle-Molina, C., Stokoe, K.H. (2012). "Seismic measurements in sand specimens with varying degrees of saturation using piezoelectric transducers." Canadian Geotechnical Journal 49 (6), 671-685.

Viggiani, G., Atkinson, J.H. (1995). "Interpretation of bender element tests." *Géotechnique*. 45(1), 149-154.

ASTM Standard D8295 – 19 (2019). "Determination of shear wave velocity and initial shear modulus in soil specimens using bender elements." ASTM International, West Conshohocken, PA. DOI: 10.1520/D8295-19.

Table 1 Properties of Georgia kaolinite clay

Parameter	Value
Liquid Limit	47
Plasticity Index	19
Specific Gravity	2.6
Slope of VCL (λ)	0.09
Slope of RCL (κ)	0.02
USCS Classification	CL

Table 2 Summary of results

Parameter	Drained heating-cooling cycle	Undrained heating-cooling cycle
Initial void ratio	1.03	1.1
Initial total density (kg/m^3)	1788	1755
Thermal axial strain after a heating-cooling cycle (%)	0.28	0.39
V_s before heating (m/s)	255.9	312.7
V_s after a heating-cooling cycle (m/s)	272.8	325.9
G_0 before heating (MPa)	122.7	180.8
G_0 after a heating-cooling cycle (MPa)	140.1	197.6
Final void ratio	0.84	0.82

List of Figure Captions

Fig. 1. Thermal triaxial system with bender elements: (a) Picture of assembled cell prior to installation of insulation around the cell; (b) Schematic of the triaxial set-up showing the internal instrumentation and the circulation system

Fig. 2. Machine deflection of the thermal triaxial system

Fig. 3. Thermo-mechanical paths: (a) Drained heating-cooling cycle; (b) Undrained heating-cooling cycle with drainage after reaching thermal equilibrium in the heating and cooling stages

Fig. 4. Typical shear wave signals obtained from bender elements in a thermal triaxial cell

Fig. 5. Changes in axial strain during heating and cooling: (a) Drained heating-cooling cycle; (b) Undrained heating-cooling cycle

Fig. 6. Excess pore water pressure during heating and cooling: (a) Drained heating-cooling cycle; (b) Undrained heating-cooling cycle

Fig. 7. Changes in thermal axial strain and excess pore water pressure with time

Fig. 8. Changes in shear wave velocity and thermal axial strain with temperature: (a) Drained heating-cooling cycle; (b) Undrained heating-cooling cycle

Fig. 9. Changes in thermal axial strain with temperature: (a) Drained heating-cooling cycle; (b) Undrained heating-cooling cycle

Fig. 10. Thermo-mechanical response of kaolinite subjected to a drained heating-cooling cycle: (a) Change in axial strain with time; (b) Axial compression curve

Fig. 11. Thermo-mechanical response of kaolinite subjected to an undrained heating-cooling cycle: (a) Change in axial strain with time; (b) Axial compression curve

Fig. 12. Compression curves replotted in terms of volumetric strain: (a) Drained heating-cooling cycle; (b) Undrained heating-cooling cycle

Fig. 13. Changes in total density of the soil specimens with temperature: (a) Drained heating-cooling cycle; (b) Undrained heating-cooling cycle

Fig. 14. Changes in small strain shear modulus and thermal volumetric strain with temperature: (a) Drained heating-cooling cycle; (b) Undrained heating-cooling cycle

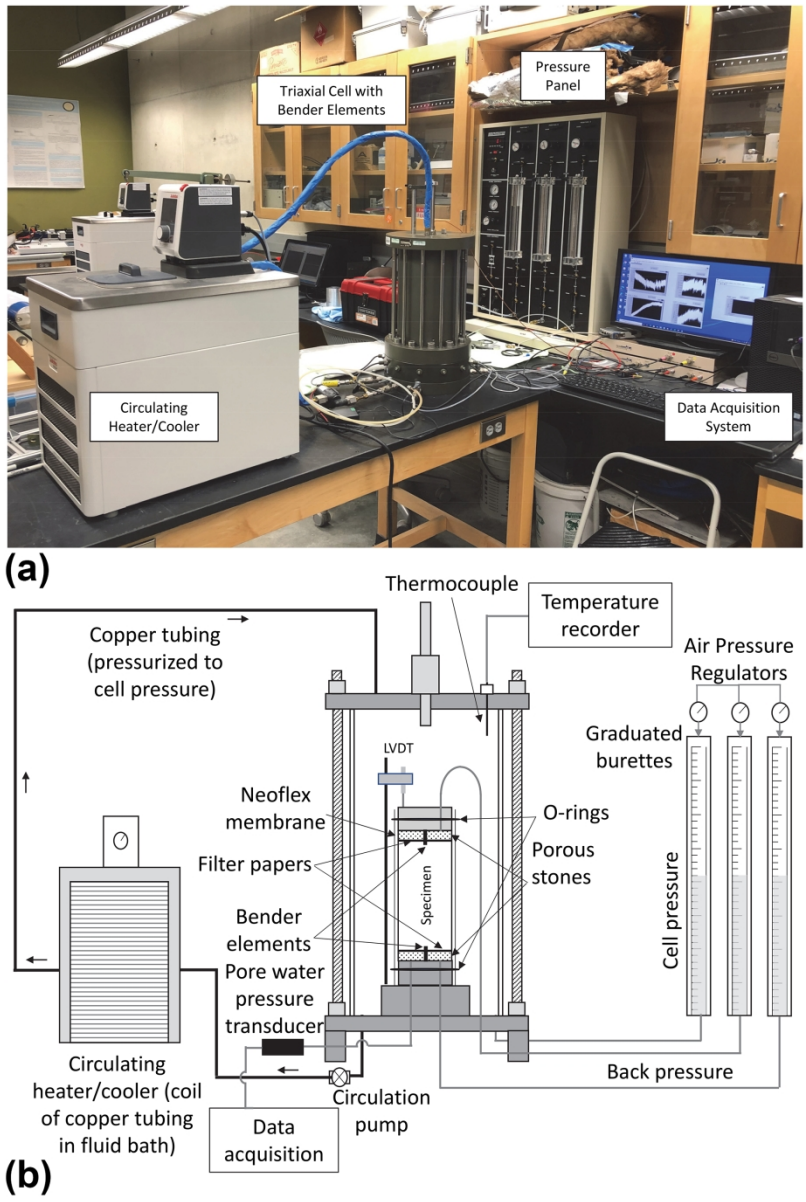

Fig. 1. Thermal triaxial system with bender elements: (a) Picture of assembled cell prior to installation of insulation around the cell; (b) Schematic of the triaxial set-up showing the internal instrumentation and the circulation system

88x132mm (600 x 600 DPI)

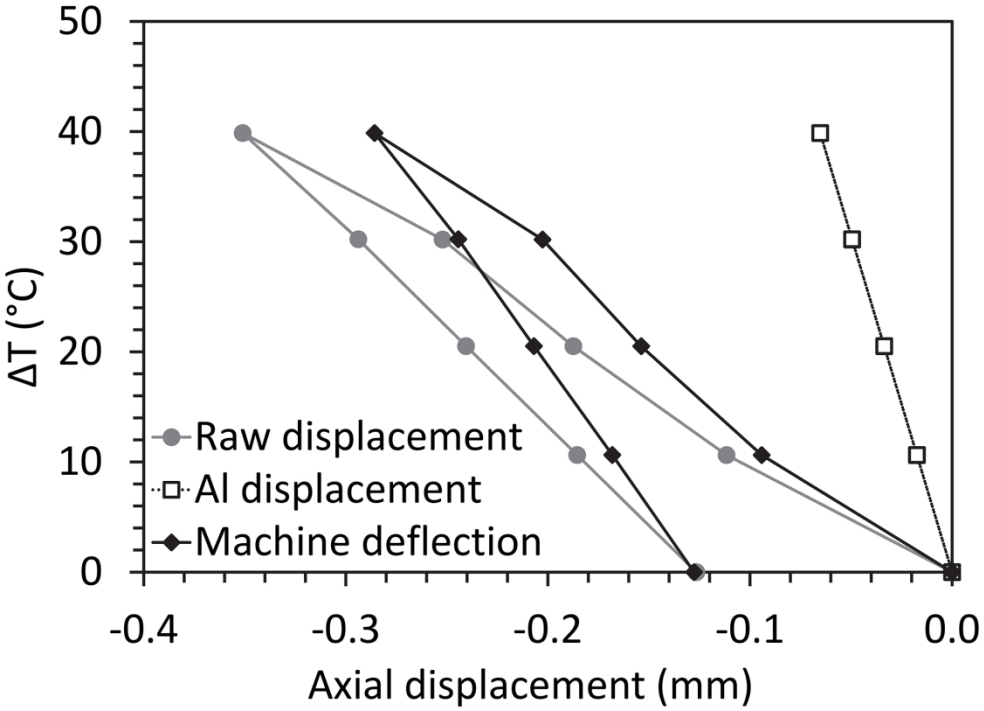

Fig. 2. Machine deflection of the thermal triaxial system

88x63mm (600 x 600 DPI)

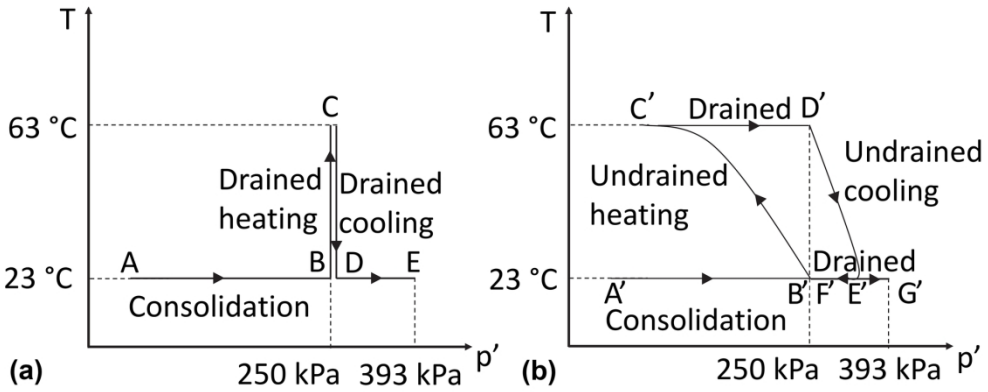

Thermo-mechanical paths: (a) Drained heating cooling cycle; (b) Undrained heating cooling cycle with drainage after reaching thermal equilibrium in the heating and cooling stages

177x70mm (300 x 300 DPI)

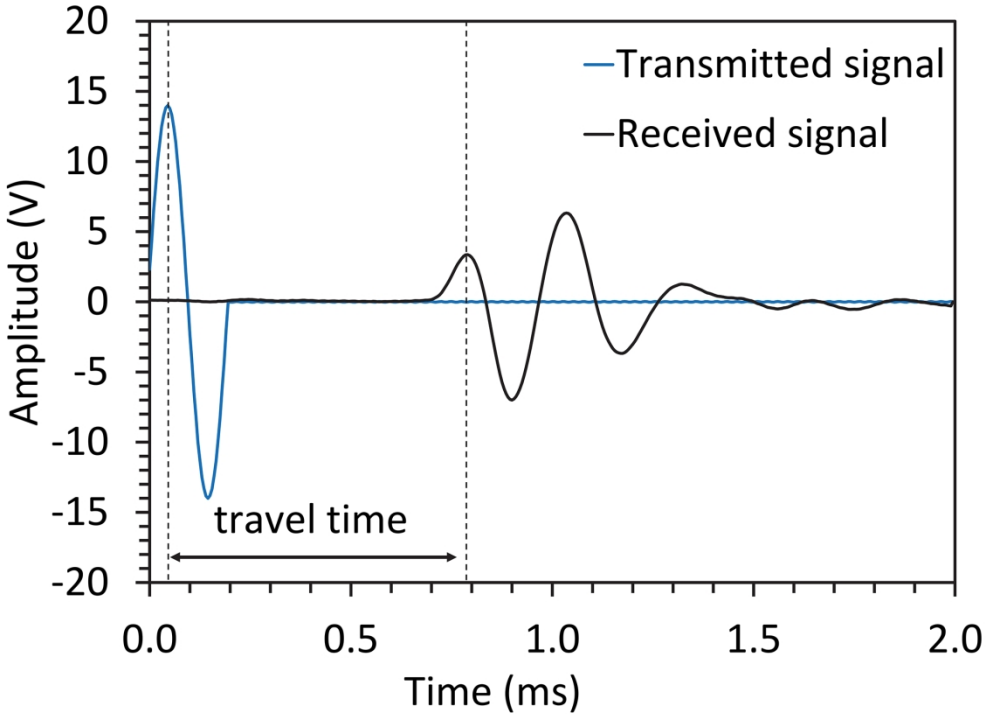

Fig. 4. Typical shear wave signals obtained from bender elements in a thermal triaxial cell

88x64mm (600 x 600 DPI)

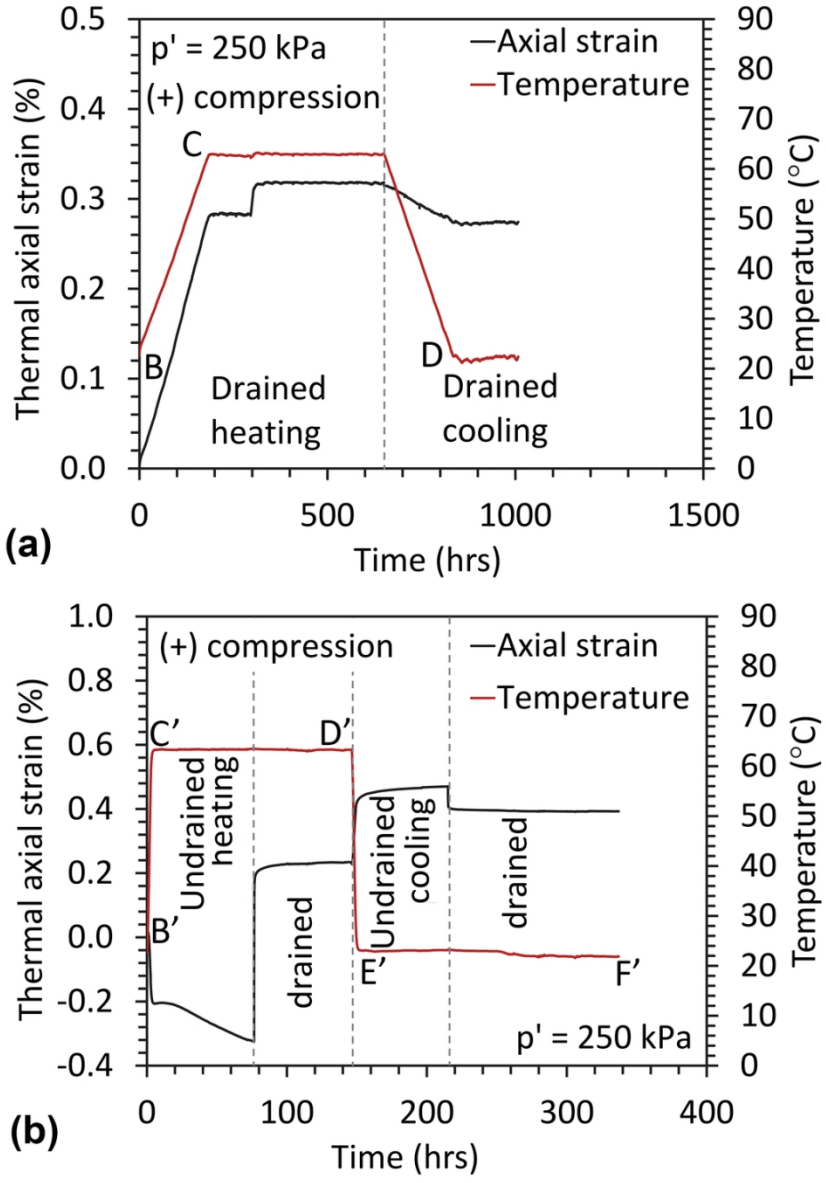

Fig. 5. Changes in axial strain during heating and cooling: (a) Drained heating-cooling cycle; (b) Undrained heating-cooling cycle

88x128mm (300 x 300 DPI)

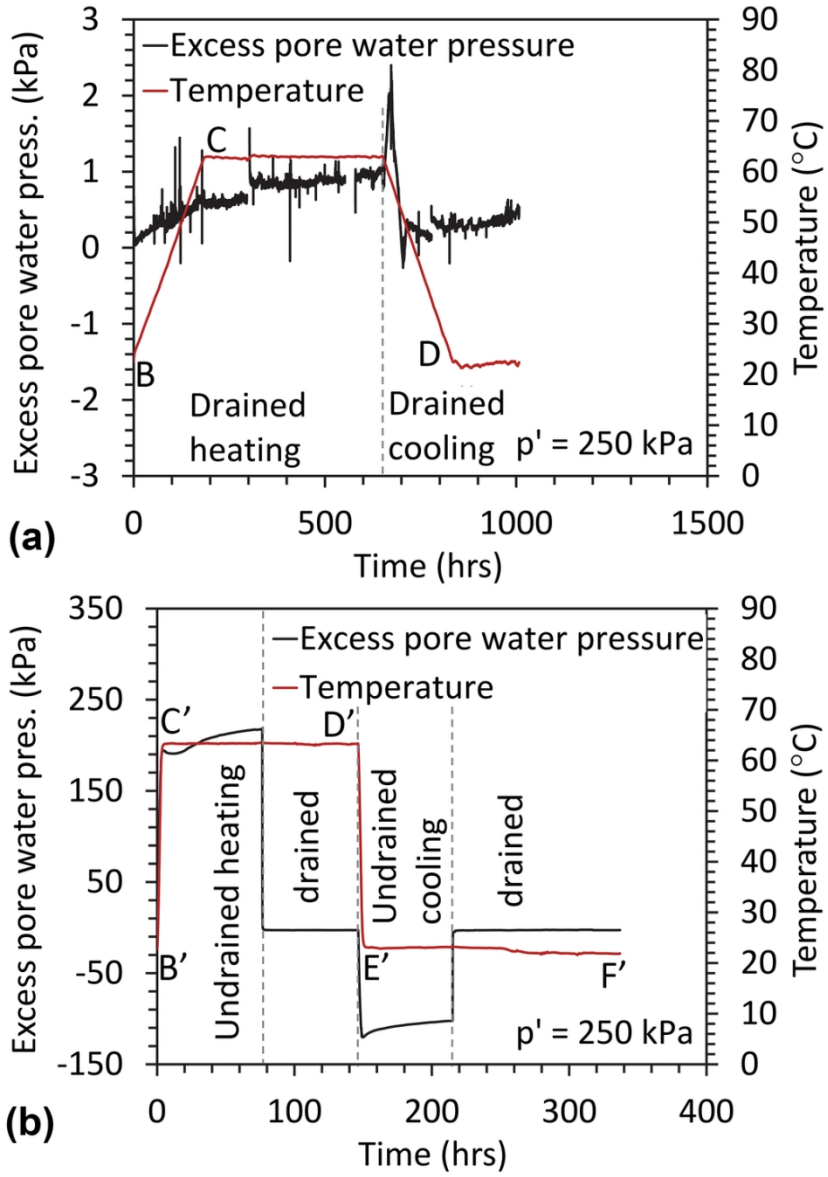

Fig. 6. Excess pore water pressure during heating and cooling: (a) Drained heating-cooling cycle; (b) Undrained heating-cooling cycle

88x127mm (300 x 300 DPI)

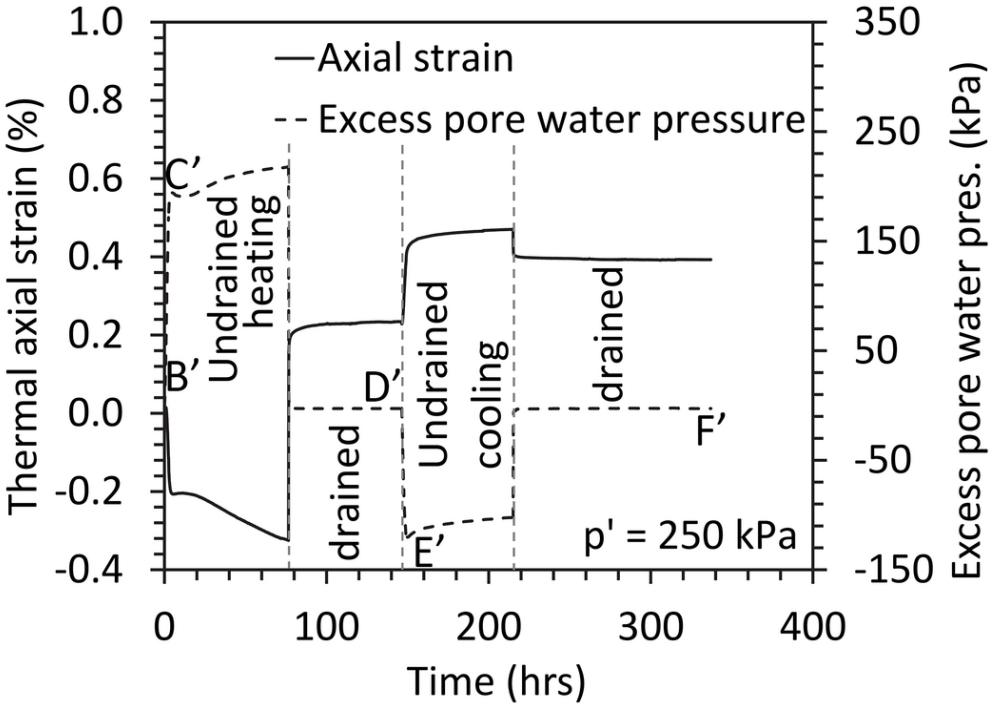

Fig. 7. Changes in thermal axial strain and excess pore water pressure with time

88x64mm (300 x 300 DPI)

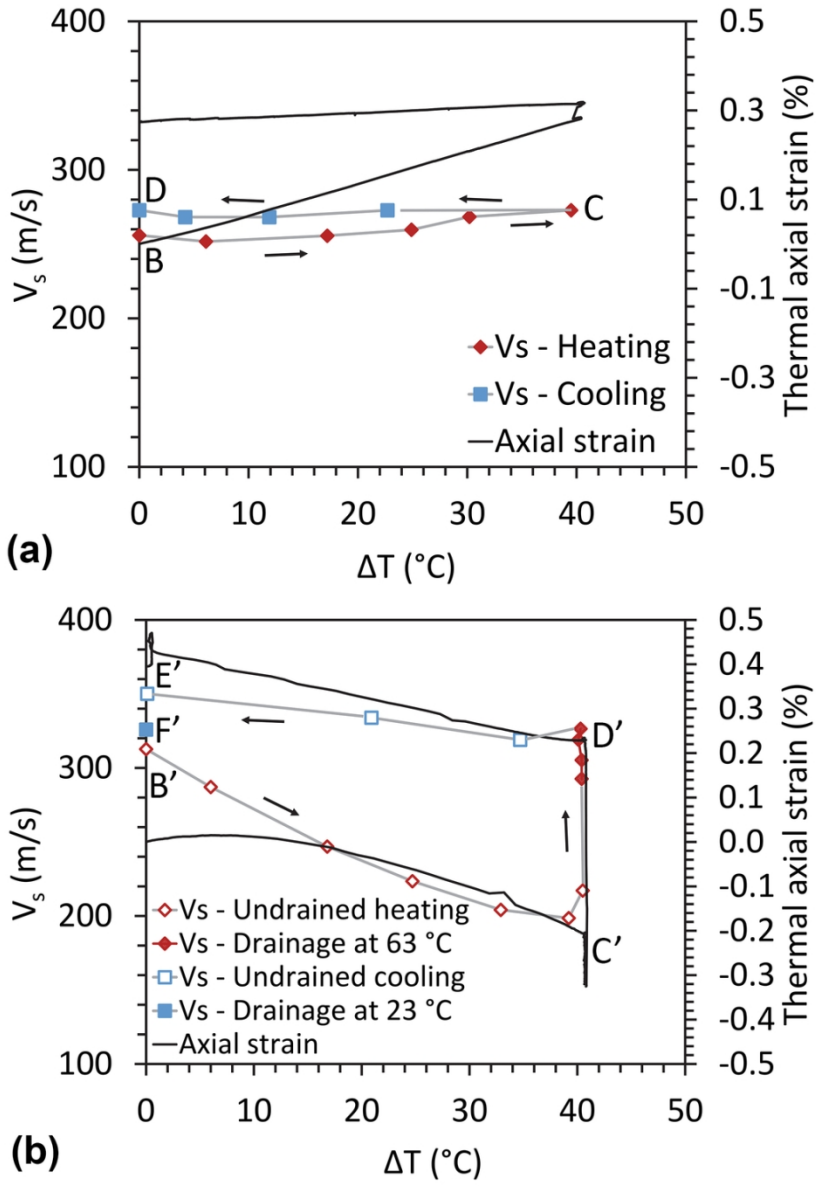

Fig. 8. Changes in shear wave velocity and thermal axial strain with temperature: (a) Drained heating-cooling cycle; (b) Undrained heating-cooling cycle

88x129mm (300 x 300 DPI)

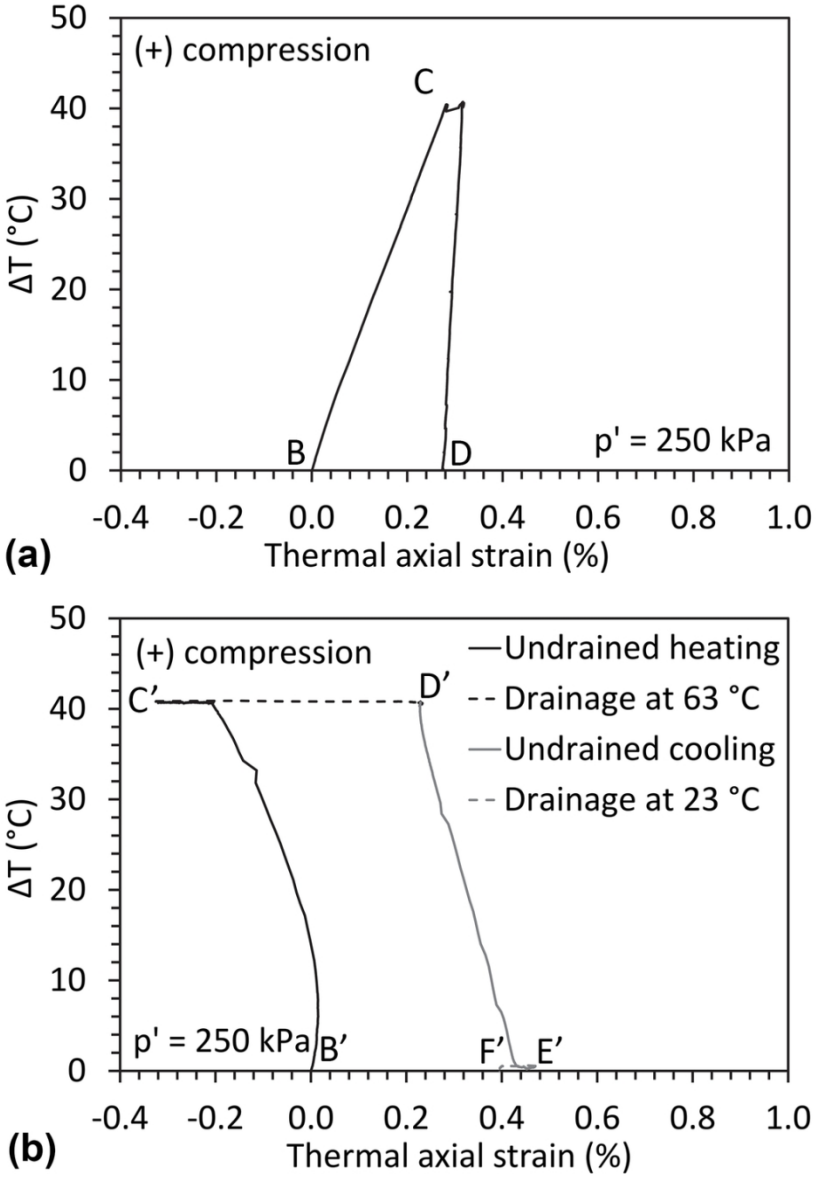

Fig. 9. Changes in thermal axial strain with temperature: (a) Drained heating-cooling cycle; (b) Undrained heating-cooling cycle

88x129mm (300 x 300 DPI)

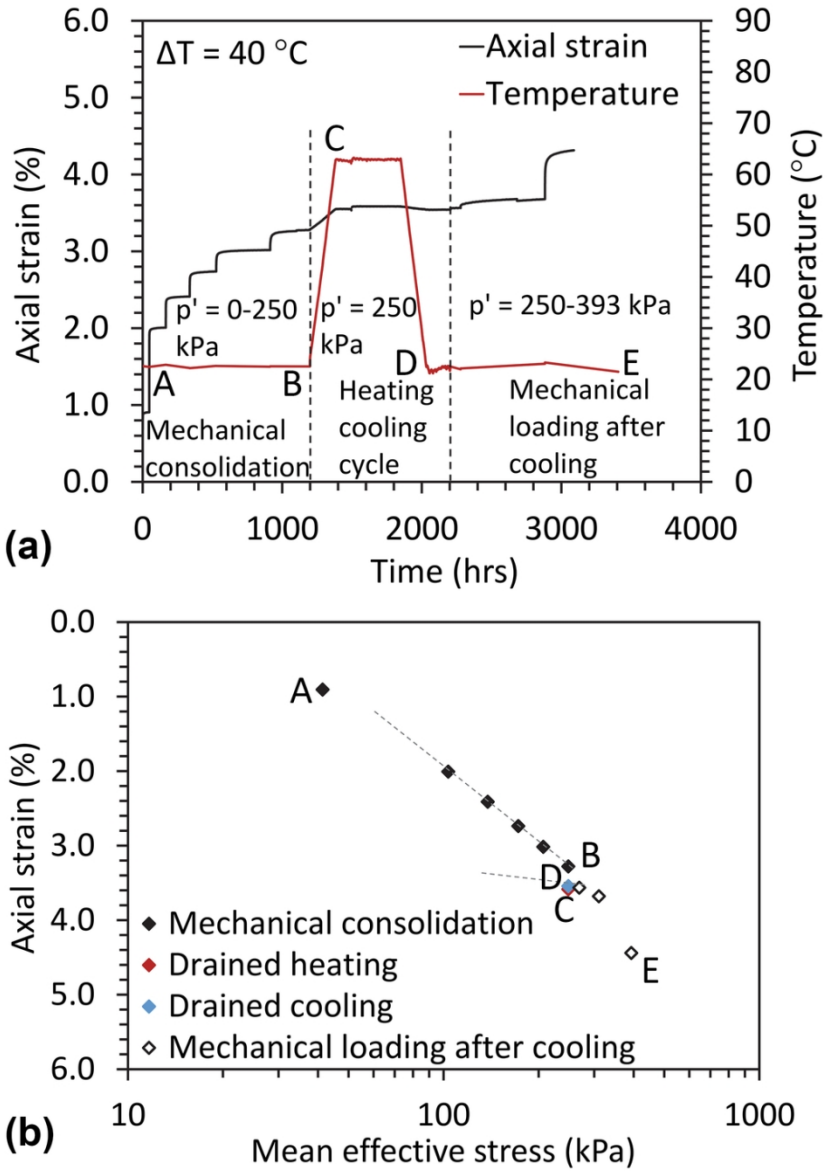

Fig. 10. Thermo-mechanical response of kaolinite subjected to a drained heating-cooling cycle: (a) Change in axial strain with time; (b) Axial compression curve

88x126mm (300 x 300 DPI)

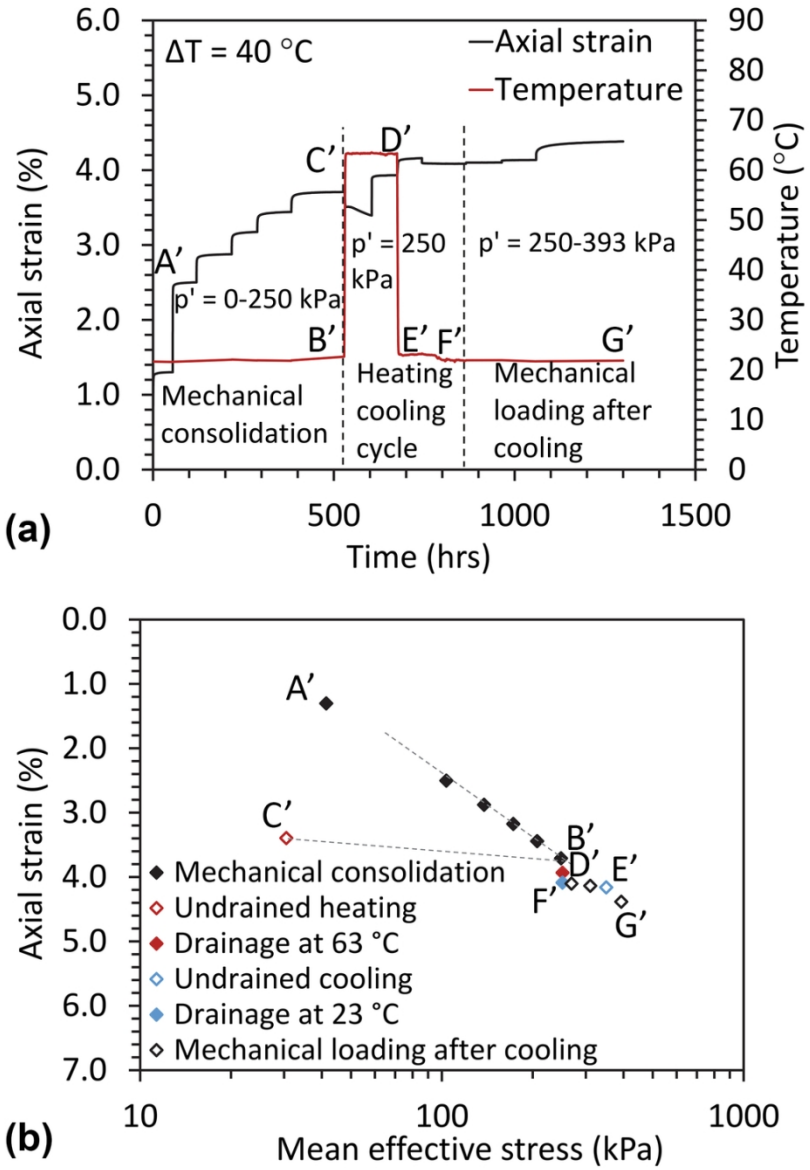

Fig. 11. Thermo-mechanical response of kaolinite subjected to an undrained heating-cooling cycle: (a) Change in axial strain with time; (b) Axial compression curve

88x130mm (300 x 300 DPI)

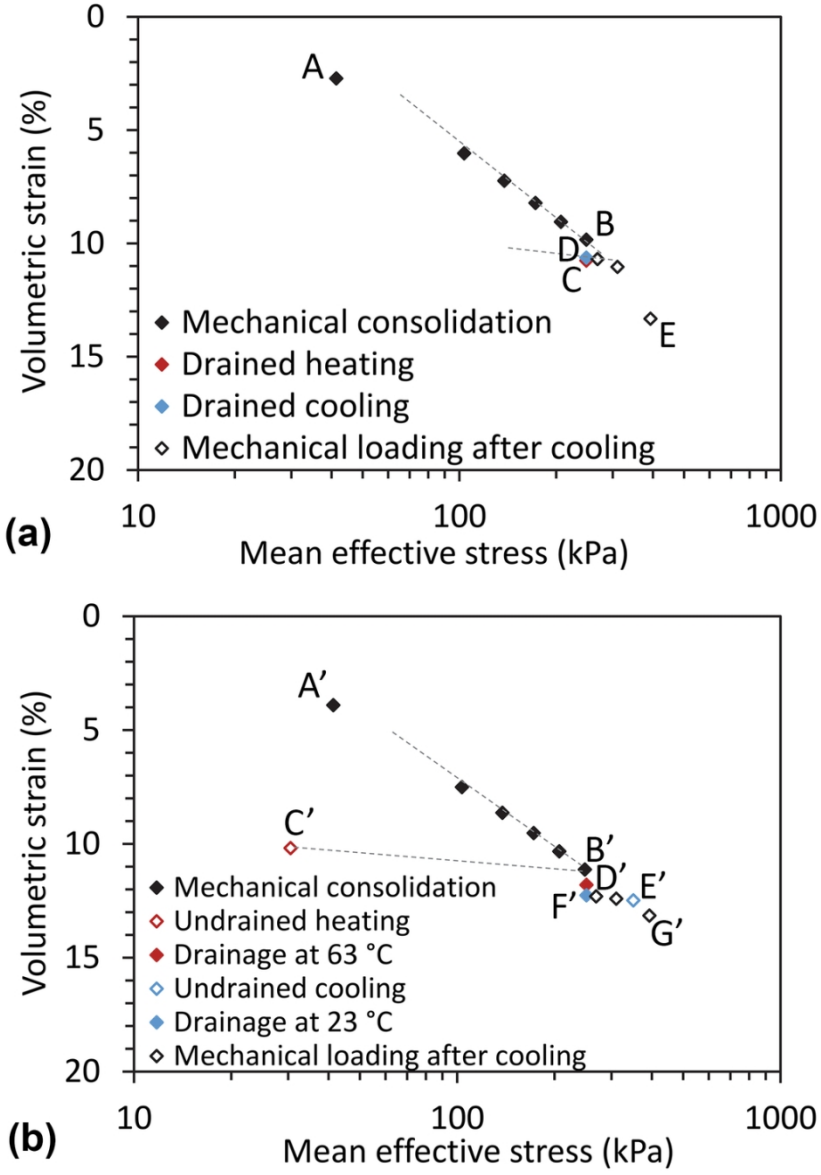

Fig. 12. Compression curves replotted in terms of volumetric strain: (a) Drained heating-cooling cycle; (b) Undrained heating-cooling cycle

88x128mm (300 x 300 DPI)

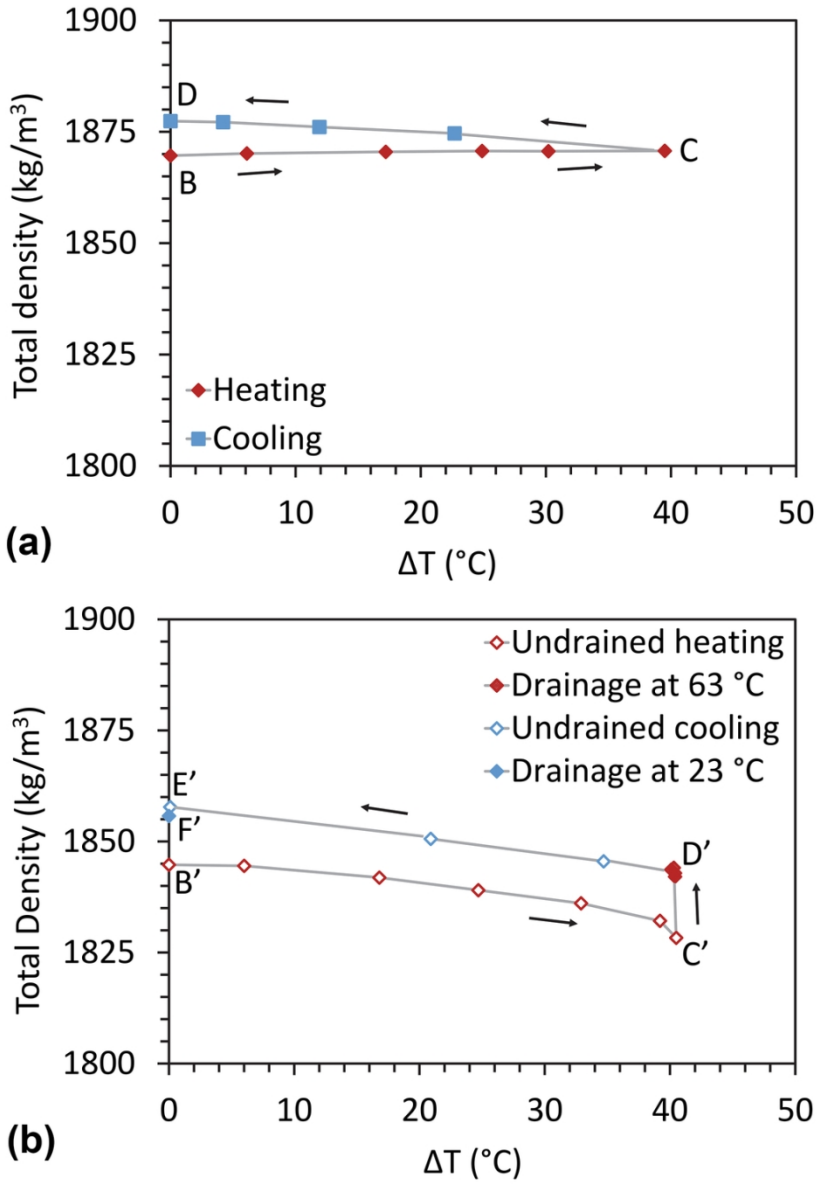

Fig. 13. Changes in total density of the soil specimens with temperature: (a) Drained heating-cooling cycle; (b) Undrained heating-cooling cycle

88x129mm (300 x 300 DPI)

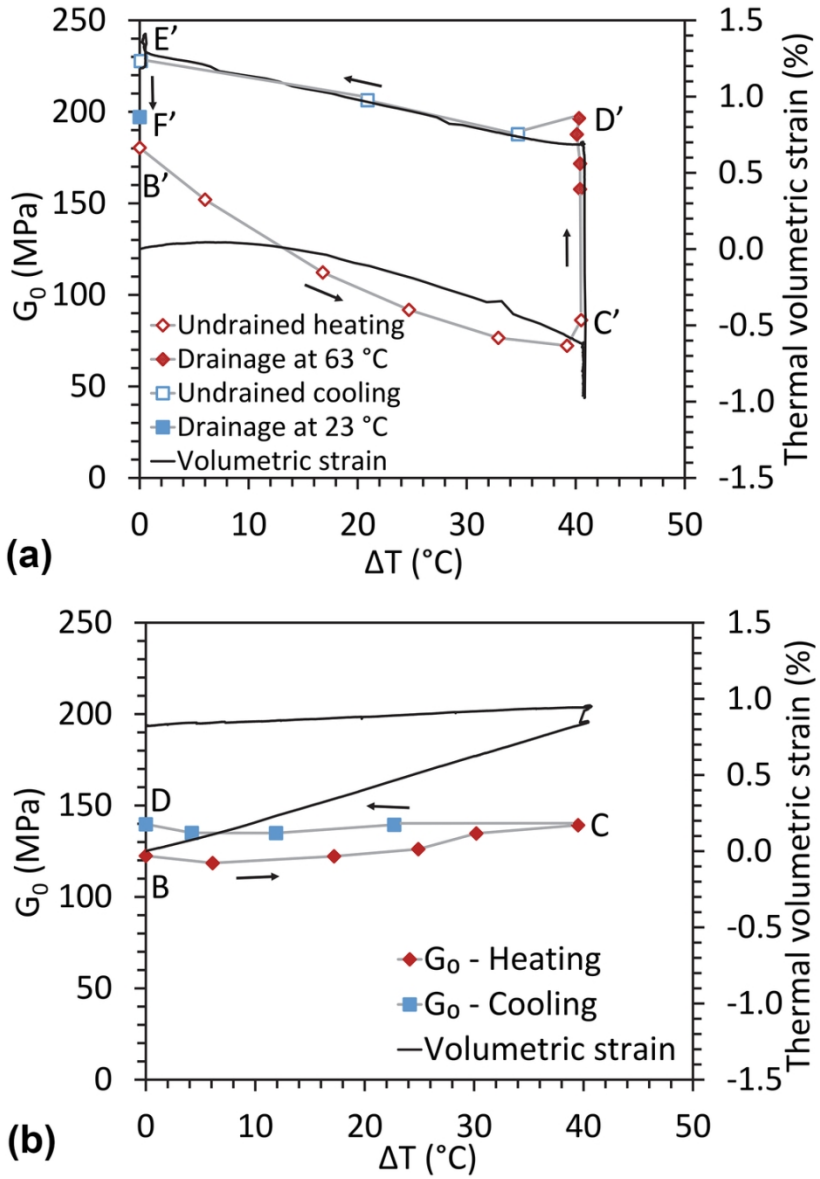

Fig. 14. Changes in small strain shear modulus and thermal volumetric strain with temperature: (a) Drained heating-cooling cycle; (b) Undrained heating-cooling cycle

88x129mm (300 x 300 DPI)